ChemistrySelect

Research Article
doi.org/10.1002/slct.202304555

Chemistry Europe
European Chemical Societies Publishing

www.chemistryselect.org

Effect of Trastuzumab and Lonidamine-Loaded Lipid Nanoparticles (LNP) on HER2+ Breast Cancer

Fatma Ozlem Zurnaci,[a, d] Sukran Ozdatli Kurtulus,[b] Ceyda Tuba Sengel Turk,[c] Canan Hascicek,[c] and Mustafa Guzel*[a, e, f]

Our study involves inhibition of glycolysis and inhibition of the HER2 pathway, which is highly expressed in many types of cancer. Decreased survival, negative metastasis, and induced apoptosis are expected due to the combined inhibition of these two targets. Trastuzumab was used as the HER2 inhibitor and lonidamine was used as the HK2 inhibitor. Lonidamine (LND) was delivered to cells as hybrid nanoparticles to enhance the effect of lonidamine and make it target specific. Separate cytotoxicity studies were conducted for LND, LND-NP and Tmab. While application of lonidamine alone gave an IC50 value of 124.6 μM, application in NP reduced the IC50 value to 44.18 μM. In addition, the combination of Tmab and LND-NP showed synergistic effects compared to treatments alone in other analyses. On the aspect of apoptosis, this combination showed a 14-fold increased apoptosis compared to the control group. This combination therapy can prevent drug resistance. In addition, the hybrid nanoparticle structure used will prevent the formation of toxicity as it will ensure that LND is administered to the body with less repetition. Our study aims to minimize the negative effects of the chemotherapy process by improving it with various variations in future studies.

1. Introduction

Breast cancer is the most common type of cancer among women in the world and has the highest mortality rate. New cases exceeded two million in 2018, although prognosis and survival rates for breast cancer have improved significantly.[1] Unlike the standard pathological features of cancers, breast cancer displays a heterogeneous disease course with various biological and morphological features. These heterogeneous structures of breast cancer make the treatment method difficult and unexpected results may occur.[2] In this context, tumor classifications are needed to strongly predict clinical outcomes.[3] When classifying breast cancer, 3 different receptors are evaluated: estrogen receptor (ER), progesterone receptor (PR), and human epidermal growth factor receptor 2 (HER2) (Figure 1). With these features of tumors, they are classified as luminal A, luminal B, HER2 positive and Triple-negative breast cancer (TNBC), and the importance of basing treatment decisions on internal molecular subtypes of breast cancer has been internationally recognized.[4] In most breast cancer cases, abnormalities in HER2 expression at the gene or protein level have been consociated with a contrary prognosis in both lymph node negative and lymph node positive breast cancer. In many different studies looking at approximately 40,000 patients, 88% of HER2 gene overexpression of the HER2 protein was found to predict breast cancer outcome in univariate or too many variables analysis.[5] The obtained data suggest that HER2 overexpression is associated with an unfavorable prognosis in node-positive and node-negative breast cancer.[6,7]

The HER2 receptor (human epidermal growth factor receptor 2) is a membrane tyrosine kinase (Figure 2). There are 4 types of membrane receptor kinases. These; HER1 (EGFR), HER3 (erbB3) and HER4 (erbB4) are receptor tyrosine kinases. These each have a transmembrane domain (an extracellular ligand binding domain), and an intracellular tyrosine kinase catalytic domain. They are transmembrane single subunit glycoproteins.[8] These receptors provide ligand activation by forming homodimers or heterodimers.[9] HER2 receptors have no known ligands to make homodimers. But it can make heterodimers with all other family members. It is similar in the activated form of RTK (Receptor Tyrosine Kinase) with the structure of the extracellular domain of HER2 without bound ligand. After the activation of these receptors, other intracellular pathways are activated, and transphosphorylations occur.[11] These pathways are Ras/mitogen-activated protein kinase pathway (mTOR), phosphatidylinositol 3 kinase (PI3 K)/Akt pathway, Janus kinase/signal converting and transcription pathway activator (JAK-STAT) and phospholipase C (PLC) pathway. As a

[a] F. Ozlem Zurnaci, M. Guzel
Istanbul Medipol University, Research Institute for Health Sciences and Technologies (SABITA), Center of Drug Discovery and Development, Kavacik-Beykoz, Istanbul 34810, Turkey
E-mail: mguzel@medipol.edu.tr

[b] S. Ozdatli Kurtulus
Department of Pharmaceutical Toxicology, University of Health Sciences, School of Pharmacy, Istanbul, Uskudar 34668, Turkey

[c] C. T. Sengel Turk, C. Hascicek
Department of Pharmaceutical Technology, Ankara University, Faculty of Pharmacy, 06560, Ankara, Turkey

[d] F. Ozlem Zurnaci
Ilkogen Biopharmaceuticals, Sanayi Mah., Teknopark Blvd., No:1/3 A/411, 34906 Pendik, Istanbul, Turkey

[e] M. Guzel
Department of Basic Pharmaceutical Sciences, Istanbul Medipol University, School of Pharmacy, 34810 Beykoz-Istanbul, Turkey

[f] M. Guzel
Department of Molecular Medicine and Biotechnology, Istanbul Medipol University, Health Sciences Institute, 34810 Beykoz-Istanbul, Turkey

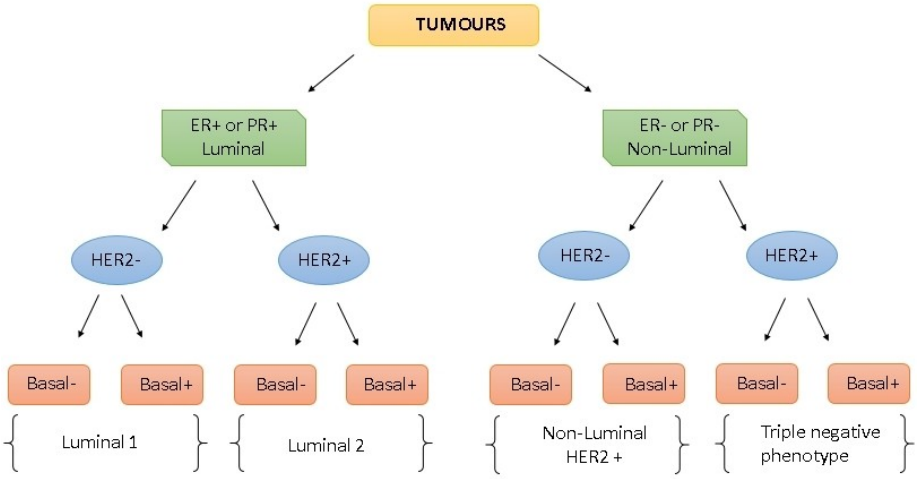

Figure 1. Molecular Classification of Breast Cancer Based on GeneExpression.

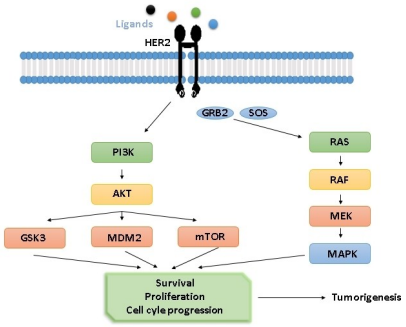

Figure 2. HER2 Receptor tyrosine kinase and its sub-pathways.

result, many actions occur such as cell proliferation, survival, cell cycle and resistance to apoptosis.[11]

HER2 overexpression is generally observed in 15% of primary breast cancers. Given the history of the disease, it has a high metastatic potential and results in decreased overall survival.[5,12] Biomarker characteristics detected in primary breast cancer may change when the tumor progresses from primary breast cancer to metastatic breast cancer.[13,14] HER2-targeted therapy reversed adverse outcomes in breast and gastric cancers that overexpress HER2 receptor tyrosine kinase.[15] HER2-targeted therapy is used in high rates of breast cancer. There are some approved treatments for adjuvant (post-surgical) and metastatic HER2-positive breast cancers. Pertuzumab (metastatic and adjuvant), Trastuzumab (Tmab) (metastatic and adjuvant), lapatinib (metastatic), ado-Trastuzumab emtansine (metastatic) and neratinib (adjuvant), in addition to these, cisplatin and a fluoropyrimidine (capecitabine or 5-fluorouracil) are used.[16,17] These treatments are also sanctioned for other HER2-positive cancer types. In addition to these treatments, Trastuzumab-dkst (Ogivri; Mylan) has been approved as a Tmab biosimilar and is used in the chemotherapy process.[17]

Tmab is a monoclonal antibody used against HER2 receptor. Tmab complementary determinant region amino acids complement amino acids located in the IVth domain of the HER2 ectodomain and binds to them. It has a very important place in the treatment of early and metastatic breast cancer. Combinations of Tmab and chemotherapy started to be used approximately 15 years ago. It has been shown to importantly high survival in HER2-positive cancer patients.[18] Tmab was administered weekly (4 mg/kg intravenous loading dose followed by 2 mg/kg IV weekly) in the first clinical trials. With subsequent studies, it has been shown that it is more appropriate to administer 6 mg/kg (with a loading dose of 8 mg/kg) every three weeks. Recorded data show that Tmab significantly improves the patients' quality of life with the introduction of chemotherapy for HER2-positive breast cancer patients.[17,20–22] (Tmab is an IgGl. Two mechanisms of function mediated by Fab, or Fc regions are proposed. Fab comprises the antigen binding sites of the antibody while Fc comprises the binding sites for Fc receptors found on immune cells, platelets, hepatocytes, and endothelial cells.[23–25] Besides the fact that Tmab provides effective treatment in HER2 positive breast cancer, long-term use of Tmab triggers the development of a resistance mechanism. As a result, cancer resistant to Tmab occur. Therefore, understanding the Tmab resistance mechanism is of great importance. The mechanisms of Tmab resistance can be examined under 4 headings (Figure 3). First, the barriers to the binding of Tmab to HER2 are the up-regulation of HER2 downstream signaling pathways, signaling via alternative pathways, and finally the inability to trigger immune-mediated mechanisms to destroy tumor cells. These models have been validated preclinically but have not yet been validated in clinical samples.[23]

Glycolysis occurs in the cytoplasm. It converts glucose into pyruvate, lactate, and hydrogen ions. As shown in Figure 4 in the first step, glucose transport is an important factor in aerobic glycolysis to protect tumor cells from high glucose consumption. The glucose transporters Glut-1 and sodium-glucose-dependent transporter 1 (SGLT1) have been found to be overexpressed in most cancer cells.[26,27] In the first step, intracellular glucose is phosphorylated to glucose-6-phosphate by the HK-2 enzyme. This product is converted to fructose-6-

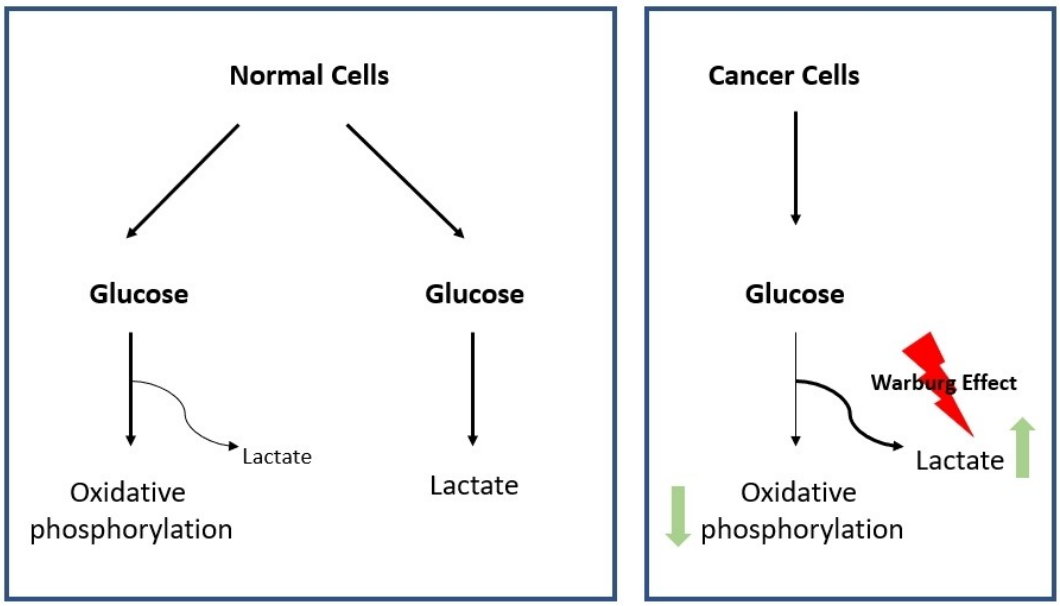

Figure 3. Biochemical transformation of glucose and Warburg Effect.

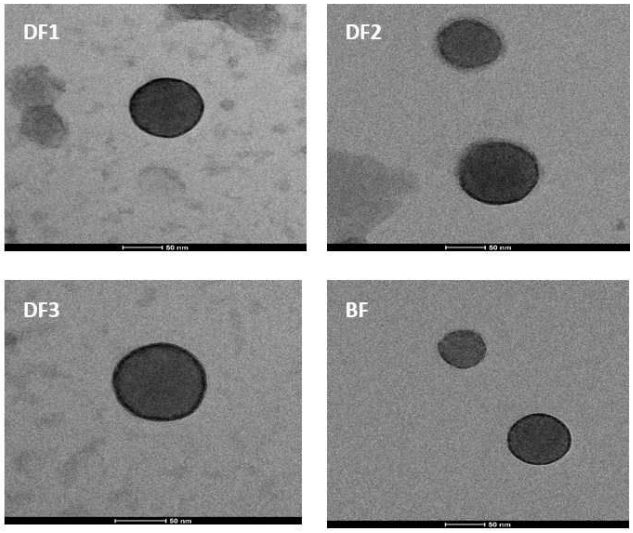

Figure 4. TEM micrographs of Ionidamine-loaded lipid-based hybrid nanoparticle formulations.

phosphate with the help of glucose-6-phosphate isomerase enzyme. Downstream of PGI modulates degradation of F-1,6-P to G6P via G6P to 6-phosphofructokinase (PFK) and fructose1,6-biphosphatase (FBPase) activities.[28] During the glycolytic pathway, F-1,6-P is converted to glyceraldehyde-3-phosphate by the enzyme aldolase (ALDO). Among the three ALDO isoforms, ALDO B is overexpressed in cancer cells.[29] In addition to ALDO, glyceraldehyde 3-phosphate can be rapidly produced from dihydroxyacetone phosphate by triosephosphate isomerase (TPI). High regulation of TPI has been reported in many cancer types. In the next step, glyceraldehyde 3-phosphate is dehydrogenated. Glyceraldehyde is converted to 1,3-bisphosphoglycerate by the enzyme phosphate dehydrogenase (GAPDH). After 1,3-bisphosphoglycerate production by GAPDH, a 1,3-bisphosphoglycerate phosphate group is transferred to ADP by phosphoglycerate kinase (PGK) to form ATP and 3-phosphoglycerate.[30,31] 3-phosphoglycerate is then converted to 2-phosphoglycerate with the help of the enzyme phosphoglycerate mutase (PGM). It is then converted to phosphoenolpyruvate by 2-phosphoglycerate enolase (ENO).[32,33] All the above-mentioned enzymes are known to be overexpressed in various cancers.[34–36]

Inhibition of glycolysis in cancer cells is associated with mitochondrial respiratory dysfunction and hypoxia. It also offers a strategy for overcoming drug resistance.[37] The development of safe and effective new therapeutic strategies depends on a better understanding of the difference between cancer cells and normal cells. One of the main biochemical features in most cancer cells is that they produce energy by increasing the rate of aerobic glycolysis. In addition, cancer cells prefer glycolysis instead of oxidative phosphorylation. Therefore, changing the shape of energy metabolism, which is a biochemical fingerprint of cancer cells, has been accepted as one of the 'characteristics of cancer. A series of cancer cell behaviors such as endless proliferation and metastasis consumes a large amount of energy. To get used to this state, cancer cells need to raise their glucose as glycolysis is less efficient than oxidative phosphorylation on adenosine triphosphate (ATP) yield. Therefore, targeting glycolysis is a promising strategy for metastatic cancer. According to new research, inhibition of glycolysis kills cancer cells. It also shows that it has a mild effect on normal cells. A single drug that inhibits glycolysis is widely used in chemotherapy.[38] The Warburg effect is associated with increased glycolysis. Therefore, there is an increase in the HK2 level. The increase of HK2 has an important place in tumor development and progression. In this context, its first step in glycolysis is the enzyme hexokinase, which controls the phosphorylation of glucose to form glucose-6-phosphate (G6P).

HK2 is an important enzyme that controls the first step of glycolysis. There are studies showing that inhibition of HK2 inhibits cancer cell proliferation without overt side effects in animal models,[39] suggesting that targeting HK2 is a viable strategy for cancer therapy.[39] The increase in HK2 enzyme level is an important difference between cancer cells and normal cells. This may lead to the development of new strategies to target and kill cancer cells.[40] Mito-HKII plays a cytoprotective role by protecting the mitochondrial membrane integrity and supports the metabolic coupling of glycolysis and oxidative phosphorylation.[41] Thus, HK2 inhibition causes a significant reduction in glycolysis, which affects multiple pathways of central metabolism and stabilizes the mitochondrial outer membrane, ultimately increasing cell death.[39]

Hexokinase 2 is an enzyme that in humans is encoded by the HK2 gene on chromosome 2. This gene encodes the enzyme hexokinase 2, the predominant form found in skeletal muscle. It is localized in the outer membrane of mitochondria48. Hexokinase (HK) converts glucose to glucose-6-phosphate (G-6-P). This G-6-P then initiates important glucose pathways including glycolysis, the pentose phosphate pathway. HK is an indispensable regulator of glucose metabolism.[42] In addition, it has been reported that increased hexokinase concentrations together with decreased glucose-6-phosphatase ratios accelerate glucose phosphorylation, resulting in increased glucose consumption.[43] Therefore, the HK family of enzymes functions to catalyze the first irreversible step of glycolysis, in which glucose is phosphorylated to glucose-6-phosphate.[44] Although HK isoforms are differentially expressed in various tissues, hexokinase 2 (HK2) is considered one of the most important subtypes for glucose metabolism in cancer cells.[45] Expression of the HK2 gene is insulin sensitive. According to studies in rats, it has been shown to play a role in increasing glycolysis in rapidly proliferating cancer cells.[46,47] In addition, the mechanism of increased glycolysis in cancer cells has been described as the Warburg effect.

HK2 is a new tumor inhibitory target. However, several potent HK2 inhibitors have been identified. Currently, 2-Deoxyglucose (2-DG) and 3-Bromopyruvate (3-BrPA), LND are the most reported HK2 inhibitors. 2-DG works as an HK2 inhibitor by replacing glucose. Since the 2-hydroxyl group is replaced with hydrogen, it cannot enter glycolysis anymore, thus stopping the glycolysis step.[38,47] As it can be understood from here, it is not a complete HK-2 inhibitor and as a single agent, it does not have an important therapeutic activity due to the dose range of 500–2000 mg/Kg in mice. As for 3-bromopyruvic acid (3-BrPA), halogenated pyruvate, and strong alkylating agent, of cysteine residues towards free SH groups in proteins, it has no use because it can affect multiple enzymes and cause inevitable side effects, is unstable, and only shows inhibition of glycolysis at high concentrations. Another drug is LND (also called TH-070).[48,49] LND, which inhibits energy metabolism in cancer cells and increases the activity of other anti-cancer agents, has been clinically studied in different cancer types such as benign prostatic hyperplasia, glioblastoma multiforme, ovarian cancer, and lung cancer, and has taken its place among supportive anti-cancer agents.[27,50] However, its use has been suspended due to toxicity problems. It seems possible to inhibit the increased glycolysis that occurs in cancer cells with the least toxicity, by developing the mechanism that LND can have a high effect at low doses.[51]

When we look at the relationship of apoptosis mechanism with HK2 inhibitors, it is at the center of the event and is at the key point for the occurrence of apoptosis.[52] HK2 mediates the ATP-mediated conversion, phosphorylation, of glucose (or other hexose sugars) to glucose-6-phosphate depending on ATP. It does this depending on the mitochondria. Mitochondrial binding helps increase selectivity as it is a property of hexokinase I and II isoforms only. HK2 binds to the mitochondrial outer membrane with high affinity. This binding is associated with the interaction with the voltage-dependent anion channel (VDAC).[53,54] According to this, binding of HK2 to the mitochondrial membrane occurs through interaction with the outer membrane protein VDAC, which activates the apoptotic process. Thus, HK2 binding to VDAC can suppress the release of its proteins into the intermembrane space and inhibit apoptosis. Thus, it may contribute to tumor cell survival.[55] When we examine this mechanism in detail, AKT can directly phosphorylate HK2. AKT also negatively regulates glycogen synthase kinase 3β (GSK3β) activity and VDAC phosphorylation. In this way, HK2 binding to mitochondria is affected. GSK3β can phosphorylate VDAC-1 on threonine 51, which allows HK2 to dissociate from VDAC-1 and affect cancer cells by chemotherapeutic agents.[56] Dissociation of HK-2 from VDAC results in disruption of the BCL-XL-BAX interaction and binding of BCL-XL to VDAC. The BCL-XL version facilitates BAX binding, which prevents BAX-BAK interaction and guards against OMM pass-through. The formation of pore structures that allow the released BAX to communicate with BAK and the release of cytochrome-c and other apoptosis proteins in the outer membrane is ensured. This leads to the initiation of apoptosis.[57]

Tumor therapy response estimation can be determined by positron emission tomography (PET) to monitor changes during therapy. 2-[18F]-Fluoro-2-deoxy-D-glucose (FDG) is the most widely used PET tracer available at all PET centers. There are many studies showing that continuous FDG-PET research in cancer patients during chemotherapy is an important method in cancer management.[58] FDG uptake is reduced within a few days of starting chemotherapy when responsive tumors are compared with pretreatment. Two studies of human tumor xenografts have produced conflicting results regarding the effect of Tmab response on FDG participation. McLarty et al. It was shown that treatment of HER-2 highly expressing MDA-MB-361 cells showed a decrease in FDG, whereas MDA-MB-231 cells that did not overexpress HER-2 showed no change in FDG regulation.[59] However, Shah et al found that FDG incorporation by Tmab-treated MMTV/HER-2 and BT474 cells was not accompanied by response.[60] As a result of these studies, some studies have revealed that inhibiting HER2 with Tmab also affects HK2. In these studies, Chenye RW et al. In his first study, Tmab not only inhibited HER2, but also stated that this inhibition decreased the expression of HK2 and accordingly FDG combination decreased.[61] Later, Smith TA et al. demon-

strated this effect with their xenograft model with mice.[62] Cooper et al. reported that the co-administration of Tmab and Metformin increased the fraction of phosphorylated [18F] FDG in cells compared to control cells, in a relationship demonstrated by previous studies, and that HK2 efficiency increased with MET.[62–64] KU004, a new quinazoline derivative molecule, with structural modification based on lapatinib, studies have been done that it is a HER2 inhibitor. The authors stated that this molecule was both an HER2 and HK2 inhibitor. However, as mentioned above, HER2 inhibition also reduces HK2 expression.[64,65] Although this drug is not an HK2 inhibitor; it has been shown that the effects of HER2 and HK2 are parallel and that inhibiting HK2 together with HER2 will have a positive effect on the tumor.

When the relationship between the HER2 receptor and the HK2 enzyme is examined in terms of apoptosis; As mentioned above, AKT is the common point of both. Therefore, both HK2 and HER2 suppress apoptosis and cause uncontrolled proliferation of cells. Inhibition of HER2 with Tmab prevents suppression of apoptosis and ensures cell death. However, resistance to Tmab prevents long-term use of the drug. It has been shown that activation of the PI3 K/AKT signaling pathway can lead to resistance to HER2-positive Tmab in this development of resistance.[66] Since AKT activation stimulates aerobic glycolysis in cancers, it is assumed that the Warburg effect may increase and lead to Tmab resistance.[67] At the same time, since AKT is involved in many vital pathways, inhibiting HK2 instead of AKT will help to induce apoptosis and increase efficiency without affecting other pathways. Targeting these two pathways together may be successful against cancer by both preventing resistance to Tmab and further inducing apoptosis.

Metformin (MET), a widely used anti-diabetic drug, has recently been the subject of research with its anti-tumor effect. In this context, in studies where Tmab and MET were given together, it was observed that when used as a neoadjuvant, it reduced the resistance and increased the success rate. Considering the mechanistic descriptions of this effect, it is thought that MET inhibits the erbB2/IGF-1 receptor.[68,69] However, recent studies on the anti-cancer mechanism of MET present evidence that it may be an HK2 inhibitor.[70,71] It is known that MET has anti-cancer properties by inhibiting HK-2 in studies performed independently of Tmab. Therefore, it is important to prevent the development of resistance and metastasis, which are among the problems encountered in the treatment of HER2 positive breast cancer patients. Also suggests that this situation may open the door to new ideas that will increase the drug efficacy by stopping the energy pathways of cancerous cells and triggering apoptosis.

In the light of these findings of KU004, we sought to investigate the synergetic effects of LND and Tmab for the treatment of solid tumors. In addition to all these, we have contributed to targeted therapy by using LND-NP in our study. Taking advantage of the nanoparticle properties rather than sending the LND to the cells in a bare state will ensure that the toxicity that may occur will be minimized. Nanoparticles have numerous intrinsic benefits over other carriers, including high drug loading efficiency, high biological environment stability, and biocompatibility, which result in superior pharmacokinetic and theragnostic drug biodistribution in clinical investigations.[72,73] As a result, nanoparticles are among the best delivery vehicles for the identification and management of a variety of cancers.[74]

Methods

Cell Culture Studies

Human breast cancer cell line, SK-BR-3 was obtained from ATCC (Manassas, VA, USA). The human HER2 positive breast cancer cell line was incubated at 37 °C, 5% CO_2. Cells were cultured in Dulbecco Modified Eagle Medium (Corning, NY, USA) supplemented with 1% Penicillin-Streptomycin, 1% non-essential amino acids and 10% fetal bovine serum (Gibco, MT, USA). During the passage, cells were washed with phosphate buffer (PBS) and incubated briefly with 0.25% (w/v) trypsin/0.53 mM EDTA (Gibco BRL) to separate them in the cell culture dish. Then 4 ml of cell medium was added to the cells and transferred to a 15 ml tube. After centrifugation at 1200 rpm for 5 min, the upper liquid in the 15 ml tube was removed. 1 ml media was added to the pellet and pipetted to suspend the cells. Cells were diluted 1:5 and transferred to a T75 cell dish and passaged every 3 days.

Preparation of Lipid Based Hybrid Nanoparticle Formulation

Nanoprecipitation technique was used to prepare LND-NP. A series of formulations were prepared using LND added at 5%, 10% and 20% (w/w) ratios of the selected poly(lactic-co-glycolic acid) (PLGA) polymer to form the polymeric core of the hybrid structure. Stock solutions were prepared by dissolving LND and PLGA polymer in acetonitrile, and 1,2-distearoyl-*sn*-glycero-3-phosphoetanolamine-*N*-carboxy(poly (ethylene glycol) (DSPE-PEG-COOH) and phosphatidylcholine were separately dissolved in a 4% ethanol-water mixture to form the lipid-based shell structure of the hybrid system. Calculated amounts of DSPE-PEG-COOH 2000 and phosphatidylcholine stock solutions were added to distilled water within the ratios presented in Table 1 and sonicated in an ultrasonic bath at 35 °C at 40 kHz ultrasonic power. The nanoparticle dispersion was centrifuged at 4500 rpm using Vivaspin 20 (Sartorius) centrifuge filters in order to remove the free excipients and uncharged drug in the environment. The obtained lipid base hybrid nanoparticle concentrate was frozen for 1 day at −80 °C and then lyophilized for 2 days (Christ gamma 2–16 LSC, Martin Christ Gef., Germany) and stored at 4 °C until use.[75] Empty nanoparticles that do not contain LND were fabricated in the same procedure (blank formulation).

Characterization of Lipid Based Hybrid Nanoparticle Formulations

Determination of Encapsulation Efficiency

In order to determine the amount of LND contained in the nanoparticles, a known quantity of lyophilized nanoparticle was sonicated in acetonitrile in an ultrasonic homogenizer for 10 min, and the amount of drug contained in the nanoparticles was determined by reading the absorbance at 298 nm wavelength in the UV spectrophotometer (n = 3). (Table 2). The encapsulation efficiency (%) values of nanoparticles were calculated using the equations given below.[76]

Table 1. Contents of lonidamine-loaded lipid-based hybrid nanoparticles.

Formula Code	Formulation Ingredients						
	Organic phase			Water phase			
	PLGA (μg)	LND (μg)	Acetonitrile (μl)	DSPE-PEG-COOH 2000 (μg)	Phosphatidylcholine (μg)	Ethanol solution (%4, (μl)	Enough amount of water (ml)
DF1	4000	200	1600	800	50	850	16
DF2	4000	400	1600	800	50	850	16
DF3	4000	800	1600	800	50	850	16
BF	4000	–	1600	800	50	850	16

Table 2. Calculations of drug loading capacity, theoretical drugamount and encapsulation efficiency.

$$\text{Drug Loading Capacity (\%)} = \frac{\text{The amount of drug in the nanoparticle}}{\text{Nanoparticle amount}} \text{X100}$$

$$\text{Theoretical Drug Amount (\%)} = \frac{\text{The amount of drug in the disperse phase}}{\text{The amount of solids in the disperse phase}} \text{X100}$$

$$\text{Encapsulation Efficiency (\%)} = \frac{\text{\% Drug loading capacity}}{\text{\% Theoretical amount of drug}} \text{X100}$$

Determination of Particle Size, Size Distribution (PDI) and Surface Charge

Photon correlation spectroscopy Zetasizer Nano ZS instrument was used to determine polydispersity index (PDI), particle sizes and zeta potential values of lipid-based nanoparticle formulations. For this purpose, analysis was made by placing nanoparticles dispersed in distilled water into the relevant chamber of the device (n = 3).

Determination of Morphological Characteristics

Transmission Electron Microscopy (TEM) analysis was used to visualize the shapes of the lipid-based hybrid formulations. For imaging purposes, hybrid nanoparticles in the form of aqueous dispersion were dropped onto the carbon film covered with copper sheet and left overnight in a petri dish with a lid and dried at room temperature. Samples prepared in this way were stained with 2% (w/v) uranyl acetate solution before being visualized.

Determination of In Vitro Drug Release Rate

Dialysis membrane technique, which is a static method, was applied to determine the release rate and release profile of LND from lipid-based hybrid nanoparticle formulations. For this purpose, nanoparticles containing 2 mg of lonidamine suspended in dialysis membranes with a molecular size of 12–14 kDa at appropriate rates were placed in 75 ml of PBS pH 7.4 phosphate buffer at 37 °C. The prepared systems were incubated in a shaker with an incubator at a rotational speed of 75 rpm (n = 3) and 1.5 ml of sample was taken at predetermined time intervals and the amount of LND released was analyzed in a UV spectrophotometer at a wavelength of 299 nm. SPSS 13.0 for Windows was utilized for the kinetically evaluation of the dissolution data of PRX (SPSS, USA).

Storage Stability

The storage stability of the lipid-based hybrid nanoparticle formulations of LND was also evaluated. For this purpose, the lyophilized form of nanoparticles was put into capped glass containers and stored at 4 °C during sixth-month periods. Entrapment efficiency, particle size, size distribution, and zeta potential were examined in this context (n = 3).

Cell Viability Analysis

The SKBR3 (HER2 positive breast cancer) cell line was cultured in high glucose medium containing 10% FBS in a 37 °C incubator with 5% CO_2. When cells covered 80% of the culture surface, they were removed using 0.25% Trypsin-EDTA (Gibco) after washing with PBS, and cells were seeded in 96-well black plates (Corning) (1×104 cells/well). After 24 h of incubation, the drug was administered in three wells for each dose to the cells that reached sufficient density. It is planned to use a total of seven control groups, including untreated cells, as controls. LND will be used as an HK2 inhibitor. The appropriate dose range to determine IC50 was determined as 400–12.5 μM as 6 doses. In the literature, LND IC50 studies are performed in 48 or 72 h, while in Tmab studies, the effective dose is given in 72 or 120 h. The IC50 value for Tmab was determined by studying 6 doses as 20–0.625 μg/ml. For LND-NP, the IC50 value was determined by studying 7 doses of 100–1.56 μM. Cell viability testing was performed using the CellTiter-Glo® Luminescent Cell Viability Assay protocol. Cell viability studies were performed in triplicate.

Annexin V Apoptosis Assay

To evaluate the viability of SKBR3 cells, eBioscience™ Annexin V Apoptosis Detection Kit FITC was used. The percentage of viable cells was determined after 48 h of incubation with Tmab, LND, LND-NP and their combinations. Annexin V studies were performed

in duplicate. The apoptosis was detected with FACS analysis. BDfacs diva machine was used.

Real-Time PCR Analysis

In logarithmic phase of growth, SKBR3 breast cancer cells were treated with Tmab, LND-NP and their combinations. Real-time PCR was performed for the determination of gene expression analysis. Primers belonging to Bax (5′- CCCGAGAGGTCTTTTTCCGAG −3′) and (5′- CCAGCCCATGATGGTTCTGAT −3′), BCL2 (5′- GGATAACG-GAGGCTGGGATG −3′) and (5′- TGACTTCACTTGTGGCCCAG −3′), and the reference gene GAPDH (5′- GGACTGACCTGCCGTCTGA 3′) and (5- TAGCCCAGGATGCCCTTGAG −3′) were used for gene expression analysis.

For the real-time PCR reaction, each experimental step was performed in triplicate and run in three biological replicates. For Syber green, reading will be made at a wavelength of 530 nm and melting curve analysis was performed to see if the amplifying gene region is replicating in the right place. The reaction was carried out by Real-time PCR instrument reading with fluorescent signals at each 0.5 °C increment between 65 °C and 95 °C.

Scratch Assay

SKBR3 cells are seeded in 6-well plates. The seeding density is adjusted to the appropriate number of cells for the SKBR3 cell line to form a confluent monolayer. The cell monolayer is drawn in a straight line with a sterile 10 μl pipette tip after 24 h of incubation. The old medium was then replaced with a medium containing the tested compounds. Plates are placed in an incubator for 48 h. After completion of the incubation, the plates are placed under the microscope to align the photographed area. Scratch assay studies were performed in duplicate. Images of the scratch were obtained. Images for each sample at 48 h were quantitatively analyzed using Image J software.

Statistical Methods

Obtained data will be expressed as mean ± SD and statistical analysis will be generated using SPSS version 21. Data will be analyzed using Tukey's post hoc test for one-way analysis of variation (One-way ANOVA) multiple comparison. P values <0.0001, <0.0003, <0.0005, <0.001, <0.005, <0.05 will be considered significant.

2. Results

2.1. Findings for Lipid-Based Nanoparticles

2.1.1. Findings for Determination of Encapsulation Efficiency, Particle Size, PDI and Surface Charge of Lipid-Based Nanoparticles

The data obtained for the encapsulation efficiency, particle size, PDI and zeta potential analyzes of the prepared lipid-based hybrid nanoparticles are presented in Table 3, arranged together with the mean value and standard error values.

2.1.2. Findings Regarding Morphological Characteristics

The micrographs obtained as a result of the TEM analysis carried out in order to determine the morphology of the LND-NP are presented in Figure 4.

2.1.3. Findings for the Determination of In Vitro Drug Release Rate

The dissolution rate profiles obtained as a result of the dissolution rate determination for LND-NP were prepared by plotting the % of drug released versus time and presented in Figure 5.

Kinetic evaluation was also performed to analyze the release rate profiles of lipid-based hybrid nano formulations more precise. The in vitro drug release data were fitted into various release models, namely zero-order, first-order and Higuchi's square root. The rate constants and statistical parameters of the kinetic models are tabulated in Table 4.

2.1.4. Findings for the Storage Stability

Storage stability of the lipid-based hybrid nano formulations were also designated at 4 °C during periods of six months. Drug content, mean particle size, PDI value, and zeta potential of the nanosystems were evaluated within this scope (Table 5).

Table 3. Physicochemical properties of lipid-based hybrid nanoparticle formulations.

Formula code	Encapsulation efficiency (%)	Average particle size (nm)	PDI	Zeta potential (mV)
DF1	81.47 ± 1.28	160.1 ± 5.71	0.121 ± 0.01	−28.9 ± 1.00
DF2	87.13 ± 1.17	175.7 ± 2.16	0.111 ± 0.03	−30.7 ± 1.05
DF3	93.89 ± 2.05	201.4 ± 5.92	0.144 ± 0.02	−31.7 ± 0.35
BF	–	147.8 ± 4.52	0.091 ± 0.03	−31.7 ± 0.72

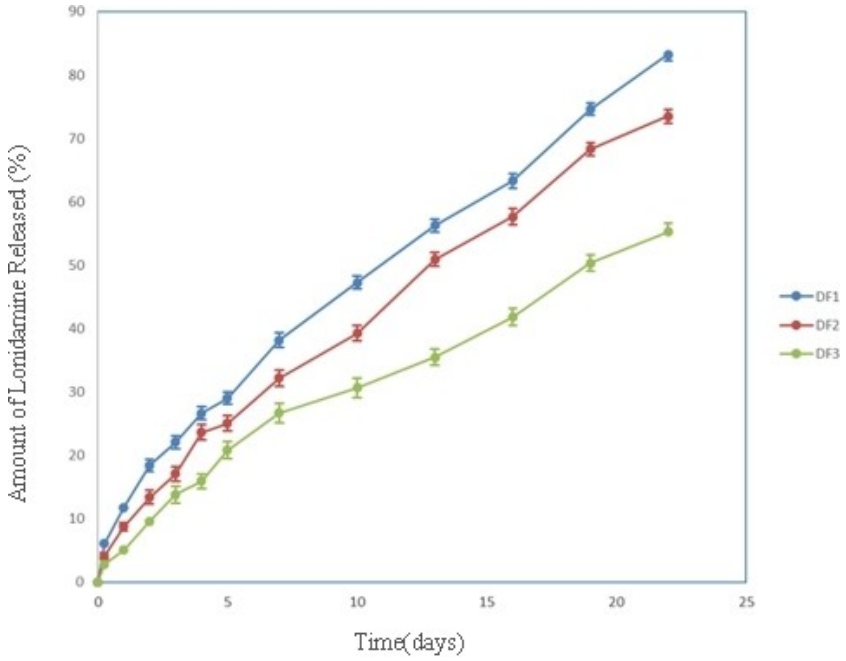

Figure 5. Dissolution rate profiles of lonidamine loaded lipid-based hybrid nanoparticle formulations.

Table 4. Kinetic evaluation data of LND release from the lipid-based hybrid nanocarrier.

Kinetic model	Rate constant	Statistics	Hybrid formulations		
			DF1	DF2	DF3
Zero-order	k_o(mg h^{-1})		15.839	9.679	2.734
		r^2	0.990	0.983	0.984
		RMS	2.979	9.128	5.342
		F_{model}	1167.068	684.928	721.525
First-order	k_1 (h^{-1})		0.096	0.182	0.109
		r^2	0.810	0.863	0.762
		RMS	21.129	42.537	52.225
		F_{model}	42.736	63.111	32.032
Higuchi	k ($h^{-1/2}$)		14.139	13.968	11.623
		r^2	0.974	0.933	0.959
		RMS	55.241	29.305	19.412
		F_{model}	457,111	480.730	567.724

RMS: Residual mean square.
r^2: Determination coefficient.

Table 5. Storage stability data of hybrid nanoparticle formulations after a storage period of six months at 4 °C.

Formula code	Encapsulation efficiency (%)	Average particle size (nm)	PDI	Zeta potential (mV)
DF1	80.23 ± 1.44	159.4 ± 4.41	0.127 ± 0.04	−27.3 ± 1.21
DF2	85.71 ± 1.38	176.2 ± 3.21	0.110 ± 0.02	−32.3 ± 1.56
DF3	94.76 ± 1.97	203.1 ± 6.75	0.138 ± 0.04	−33.8 ± 1.74

2.2. Cell Viability Analysis

To investigate the effects of LND, Tmab, LND-NP, and Blank NP on cell viability in the SKBR3 HER2 positive breast cancer cell line, cells were exposed to the drug. Afterward, cell viability was measured using the CellTiter Glo experiment kit, which is a kit based on the determination of the amount of ATP in the medium.

As seen in the graphs above, LND, LND-NP, blank-NP and Tmab(72 h,120 h) gave IC_{50} values of 124.6 μM, 44.18 μM, 210.1 μM, 9.5 μg/ml and 1.12 μg/ml, respectively (Figure 6). IC50 studies were performed in triplicate.

2.3. Annexin V Results

The flow cytometry results, performed in duplicates, showed that among the drug treatments, LND-NP and Tmab combination had the highest effect on apoptosis induction after 48 h incubation on SKBR3 cells ($p < 0.0001$) (Figure 7).

When the Annexin V images were examined, the combination of LND-NP and Tmab expressed with g significantly led SKBR3 cells to apoptosis. The graphic below shows the statistical analysis of all groups and combinations.(Figures 8 and 9).

Measurements of late apoptosis were calculated by proportioning them with the control group. According to this, control group 100 ± 0, Tmab group 125 ± 2.122, LND group 104.0 ± 0.1131, LND-NP group 529.6 ± 27.45, blank NP group 192.1 ± 5.433, Tmab-LND group 238.0 ± 1.075, Tmab-LND NP group 1418 ± 31.63 was calculated. Annexin V studies were performed in duplicate.

LND-NP significantly induced cells to apoptosis when compared between all doses and combinations. The combination of LND-NP and Tmab showed a synergistic effect. After 48 h of drug exposure, the percentage of cells leading to late apoptosis and the percentage of dead cells increased significantly. In addition, empty nanoparticle structures encoded as Blank-NP showed a significant effect in cells.

2.4. Real Time PCR Analysis

Real-time PCR was used to assess the expression levels of BAX, BCL-2 gene in breast cancer. In all assessments, untreated cells were used as negative controls. All the experiments were carried out in triplicates.

Measurements of BAX/BCL-2 ratio were calculated by proportioning them with the control group. According to this, control group 1 ± 0, Tmab group 0.9352 ± 0.006, LND group 5.123 ± 0.010, LND-NP group 1.194 ± 0.007, blank NP group 1.75 ± 0.07, Tmab-LND group 3.733 ± 0.094, Tmab-LND NP group 15.37 ± 0.1162 were calculated. Scratch assay studies were performed in duplicate.

According to the Real-Time PCR results, the BAX/BCL-2 ratio was compatible with the other apoptosis data. Especially when only Tmab and LND NP are examined, there is a low rate, while the combination of the two drugs creates a synergistic effect and gives a significant BAX/BCL-2 ratio.

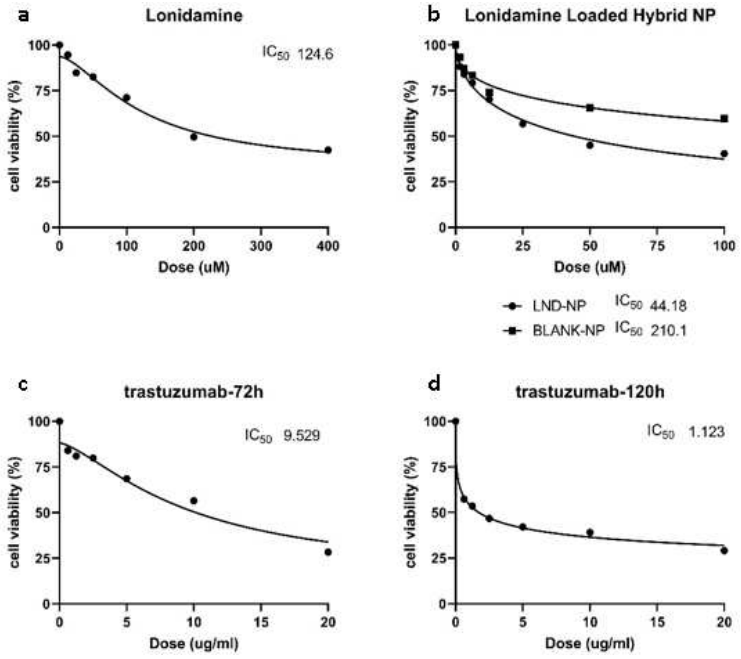

Figure 6. Determination of IC50 values of drugs and drug delivery system used in the study. a; Lonidamine(48 h), b; Lonidamine-NP and Blank-NP (48 h), c; Tmab(72 h), d; Tmab(120 h).

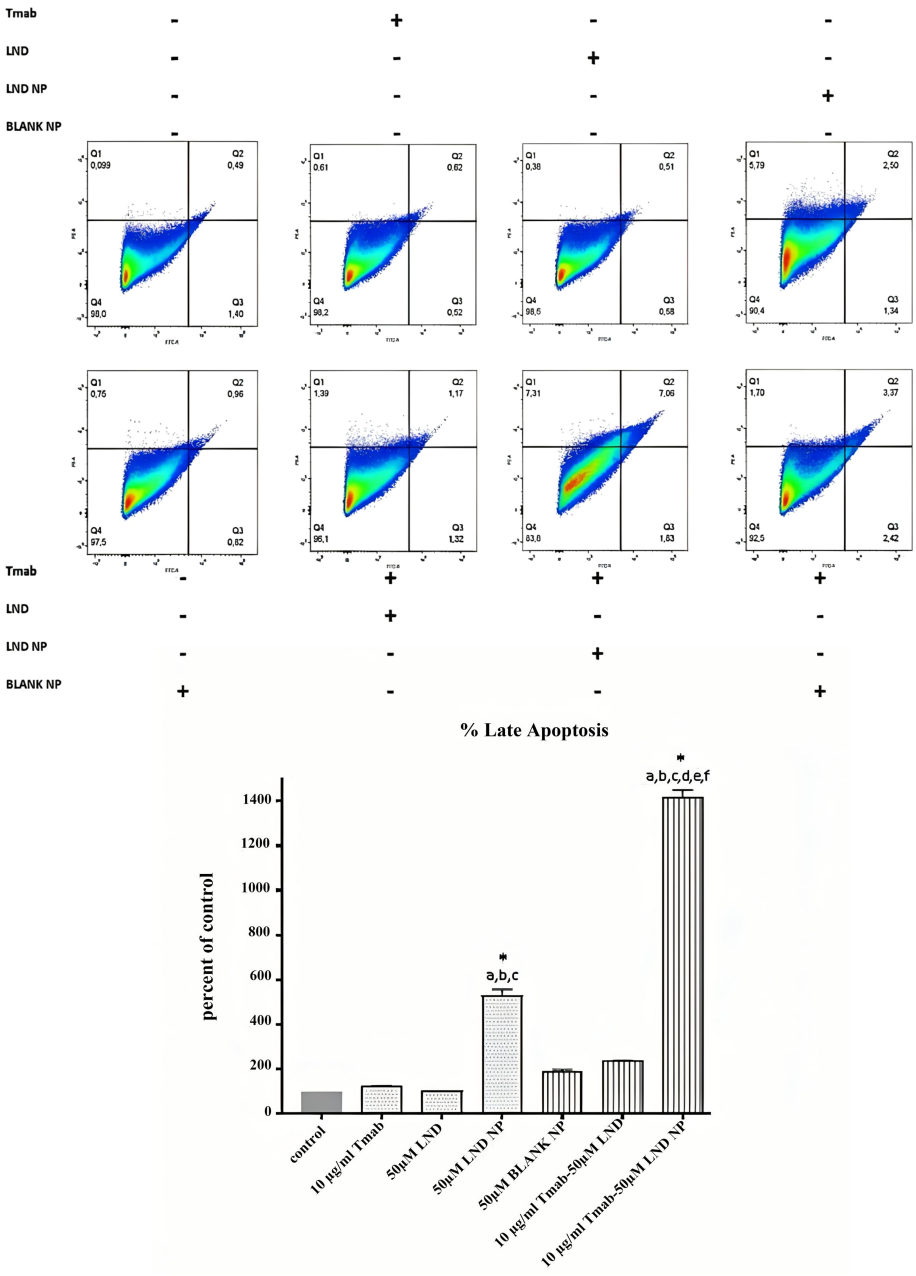

Figure 7. Flow cytometry analysis of cancer SKBR3 cells after 48 h treatment with Lonidamine, Lonidamine-NP, blank-NP, Tmab and its combinations. Cells considered viable are Annexin V and PI negative. Statistical analysis of Annexin V results. The results were expressed as the mean of duplicates ± SD. Cells treated with control, LND (50 µM), LND-NP (50 µM), blank-NP (50 µM) and Tmab (10 µg/ml) (*$p < 0.0001$). *a significantly different from control, *b significantly different from Tmab, *c significantly different from LND, *d significantly different from 50 LND-NP, *e significantly different from blank-NP, *f significantly different from Tmab-LND combination

2.5. Scratch Assay

According to the Scratch Assay images and statistical evaluation, treatment with Tmab, LND and LND NP significantly inhibits the migration of cells. Combination groups significantly increase the wound area compared to drugs applied alone. In addition, the combination of Tmab and LND NP significantly increases the wound area compared to the combination in which Tmab and LND are applied together.

Measurements of wound area were calculated by proportioning them with the control group. According to this, control group 1657 ± 204.6, Tmab group 2698 ± 268.1, LND group 2764 ± 311.4, LND-NP group 4100 ± 438.9, blank NP group 1438 ± 146.5, Tmab-LND group 3632 ± 276.6, Tmab-LND NP group 5386 ± 185.1 were calculated.

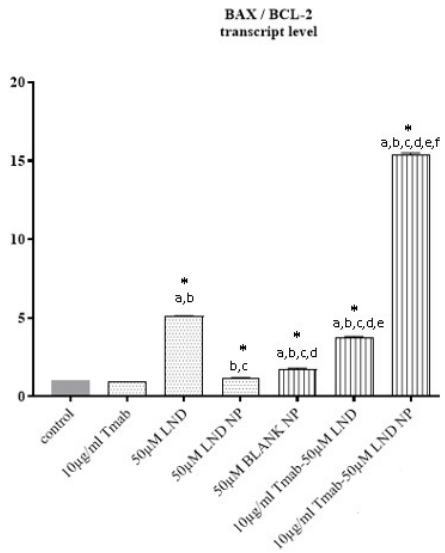

Figure 8. BAX/BCL-2 ratio. The results were expressed as the mean of triplicates ± SD. Cells treated with control, LND (50 μM), LND-NP (50 μM), blank-NP (50 μM) and Tmab (10 μg/ml) (*$p < 0.0001$). *a significantly different from control, *b significantly different from Tmab, *c significantly different from LND, *d significantly different from 50 LND-NP, *e significantly different from blank-NP, *f significantly different from Tmab-LND combination.

3. Discussion

Our study explains the targeting of two pathways and the effect of combined treatment in order to contribute to the chemotherapy process of HER2 positive breast cancer patients. As it is known, combined therapies can produce synergistic effects by targeting more than one pathway instead of a single target. It can also be useful in preventing drug-induced resistance by targeting both pathways. Recently, it has been seen that inhibiting the energy pathways of cancer cells gives successful results in cancer treatment. It has been determined that the glycolysis pathway, which is the first step of the energy production process, is over-activated in many cancer types. In this context, the Warburg effect is remarkable in cancer cells. The Warburg effect is the observation that most cancer cells release energy predominantly through a less efficient process of glycolysis, rather than through the 'usual' citric acid cycle and oxidative phosphorylation in the mitochondria as observed in normal cells. In this study, we set the target to inhibit the glycolysis pathway by targeting the HK2 enzyme. The HER2 receptor protein, a tyrosine kinase protein, is overexpressed in some cancer cells. This results in increased survival, proliferation, and metastasis. We aimed to inhibit these two target pathways by using LND as HK2 enzyme inhibitor and Tmab as HER2 receptor inhibitor and to observe the effectiveness on cell survival, apoptosis, and proliferation. Although Tmab is currently used in chemotherapy, it shows drug resistance in long-term use. Although LND has been shown to be effective in clinical practice, its use is limited due to its toxic effects. By targeting these two pathways, it is expected that more than one death mechanism will be stimulated, and a synergistic effect will occur.

The encapsulation efficiency values of lipid-based hybrid nanoparticle formulations loaded with LND were determined in a narrow range of 81.47%–93.89%. The encapsulation efficiency values of the prepared formulations increased statistically as the particle sizes of the nanoparticles increased ($p < 0.05$). This situation was realized by the increase in the viscosity of the organic phase due to the increase in the ratio of active substance in this phase, and thus the higher level of LND loading on the nanoparticles due to the increase in the particle size of the nanoparticles[77,78] (Table 3). The viscosity values of the organic phase of the DF1, DF2 and DF3 coded formulations were found as 18.3 cP, 27.9 cP and 41.5 cP, respectively. These values have proved our interpretation.

When the particle size values of lipid-loaded hybrid nanoparticle formulations containing LND in different ratios (5–10% and 20% of the polymer) are examined in terms of formulations containing and without active ingredient, the particle sizes of formulations containing LND are primarily determined in the range of 160.1 nm–201.4 nm ($p < 0.05$) The particle size of the empty nanoparticle formulation without LND was determined as 147.8 nm. It was determined that the particle sizes of the formulations containing LND increased statistically significantly depending on the increase in the active substance content. It is thought that this is due to the increase in the viscosity of the organic phase, resulting in the formation of a more viscous organic phase that is more difficult to disperse in the water phase during sonication, and it has been determined that an increase in particle size is observed in this way.[78,79] The particle size of the empty formulation without LND was determined as 147.8 nm and it was determined that there was a statistically significant reduction in the particle size since the active ingredient was not included in the formulation content ($p > 0.05$) (Table 3).

When the PDI values of the developed lipid-based hybrid nanoparticle formulations were examined, it was determined that the particle size distributions were determined in a narrow range based on all the formulations prepared ($PDI < 0.2$) (Table 3).[78]

The indicator of the stability of nanoparticles in the dispersion medium is the zeta potential value. The higher the zeta potential, the greater the repulsive forces between the nanoparticles. Thus, the aggregation of nanoparticles in the dispersion medium is prevented and the high stability is ensured. When the zeta potential values of the prepared lipid-based hybrid nanoparticle formulations were examined, it was stated that the nanoparticles had a negative surface charge in the range of −28.9 mV–−31.7 mV. This situation indicated that the stability of all nanoparticle formulations was high (Table 3).

It was determined that the lipid-based hybrid nanoparticle formulations prepared within the scope of this research could be obtained in a spherical shape and it was designated that the phospholipid shell wall of the nanoparticles could be observed clearly.

When the release rate of LND from the developed lipid-based hybrid nanoparticles was evaluated over the active substance ratio, it was stated that the release profiles were proportional to the varying particle sizes ($p < 0.05$) (Figure 5). As

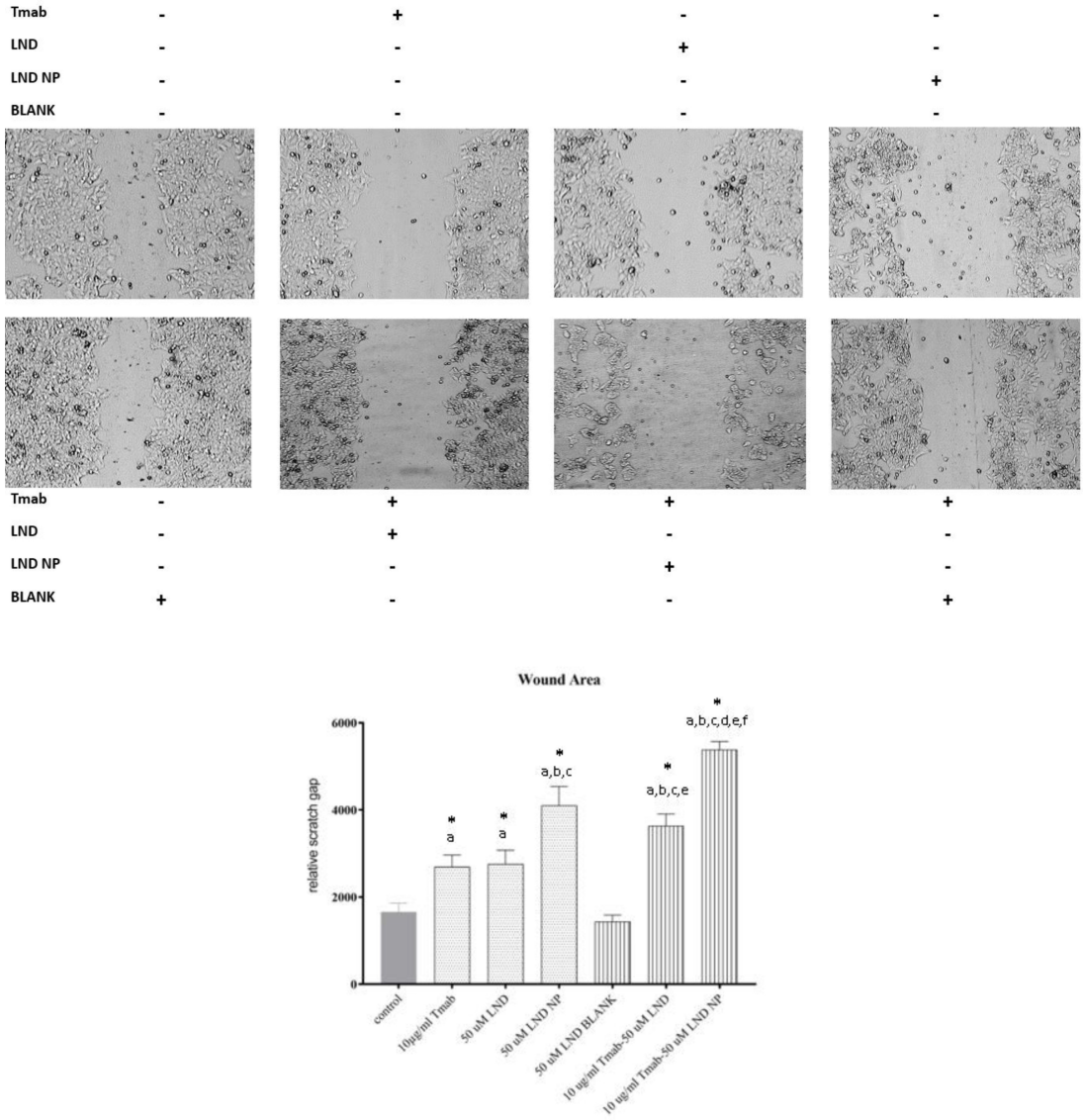

Figure 9. Representative images of scratch assay. Statistical analysis of the scratch assay. The results were expressed as the mean of triplicates ± SD. Cells treated with control, LND (50 uM), LND-NP (50 μM), blank-NP (50 μM) and Tmab (10 μg/ml) (*$p < 0.0001$). *a significantly different from control, *b significantly different from Tmab, *c significantly different from LND, *d significantly different from 50 LND-NP, *e significantly different from blank-NP, *f significantly different from Tmab-LND combination.

a result of in-vitro release rate studies carried out for 22 days, it was observed that approximately 55.27%–83.21% of LND was released from the formulations developed. During this period, the highest release of active substance from the lipid-based hybrid nanoparticle systems was achieved in the DF1 coded formulation. Cell-based experiments were continued with DF1 encoded lipid-based hybrid nanoparticles.

The kinetic evaluation of the dissolution release data was carried out according to the lowest RMS value and the highest determination coefficient and the F value, which represents the fit to the model. When the in vitro drug release data of LND from the lipid-based hybrid nanocarriers were fitted to stated kinetic models, it was observed that the all formulations complied with zero order kinetic, which is an indicator of controlled release manner (Table 4). When the zero-order kinetic rate constants of all formulations are compared with each other, the finding that the fastest release is observed in the DF1 coded formulation is proven.

Statistical evaluation of the drug content stability data indicated that the developed lipid-based hybrid nano formulations qualified as active compounds without any changes, and also demonstrated excellent chemical stability for entrapped lonidamine ($p > 0.05$). The measurements of size distribution, mean particle diameter and surface charge of the nanoparticles revealed no changes for any of the formulations after a storage period of six months at 4 °C ($p > 0.05$).

As a result of all in vitro characterization studies, among the LND encapsulated hybrid nanocarriers, DF1 encoded lipid-based hybrid formulation was chosen as the final formulation for cell-based experiments.

Firstly, IC50 doses of Tmab, LND, and LND loaded hybrid NP were determined in SKBR3 cells. Since Tmab is an antibody and shows activity by binding to a receptor, long-term treatment is required. In this context, studies in the literature were generally carried out between 120 h and 72 h.[67,80–84] LND and LND NP IC50 values were evaluated as 48 h. According to the results obtained, Tmab 72 h gave 9.5 μg/ml, Tmab 120 h 1.12 μg/ml, LND 48 h 125 μM and LND NP 45 μM IC50 values (Figure 6). The results of both LND and Tmab IC50 overlap with the literature studies.[85–87] There is no LND and Tmab combination study in the literature. In this context, our work has original value. The results clearly indicate that there is a synergistic effect of both LND and Tmab combination for cancer therapy. Additionally, the more effective LND analogs which are under development in our labs might demonstrate more potential synergy as well as stand-alone cancer treatment.

The positron emission tomography (PET), which is used to observe the change in tumor tissue, is based on the inclusion of the marked isotope 2-[18F]-Fluoro-2-deoxy-D-glucose (FDG). In general, responsive tumors show a reduction in FDG uptake within a few days of starting chemotherapy compared to pretreatment. It has been shown that there is a decrease in FDG uptake after Tmab in the treatment of HER2 breast cancer. Studies have revealed that inhibiting HER2 with Tmab also affects HK2. In the first study by Chenye RW et al., Tmab not only inhibited HER2, but also stated that this inhibition decreased the expression of HK2 and accordingly, FDG combination was also decreased.[61] Later, Smith TA et al. demonstrated this effect with their xenograft model with mice. Tian C *et al.*, is a new quinazoline derivative molecule with structural modification based on lapatinib named KU004. Studies have been done showing that this molecule is an HER2 inhibitor and later stated that this molecule is both a HER2 and HK2 inhibitor. As we mentioned above, HER2 inhibition also reduces HK2 expression.[65,87] The formation of this effect may be due to the interaction of HER2 receptor and HK2 with each other via the AKT-PI3 K pathway. In our study, the effects on cell growth and proliferation were investigated by inhibiting HER2 and HK2, whose expression is increased in cancer cells. In this context, according to Annexin V/PI analyzes after 48 h of exposure, cell viability was 98% in control, 97% in 10 μg/ml Tmab and 50 μM LND, 90% cell viability and 2.5% late apoptosis in 50 μM LND loaded NP, In the combination of 10 μg/ml Tmab + 50 μM LND loaded NP, cell viability was 83.8%, late apoptosis was 7.06% and dead cell percentage was 7.31%. According to these results, it is clearly seen that LND loaded hybrid NPs direct cells to apoptosis. In addition, the Tmab-LND loaded NP combination appears to be much more effective than the groups in which drugs are administered alone, by creating a synergistic effect. There are studies showing that when LND and Tmab drugs are given as monotherapy, they cause cell death and even stimulate apoptosis.[88–93]

Many mechanisms play a role in the formation of apoptosis. Proteins linked to the BCL-2 family maintain the integrity of the mitochondria and are key regulators of mitochondria-initiated caspase activation. Some proteins belonging to this family can act as antiapoptotic (BCL-2, BCL-XL, etc.) and some proteins as proapoptotic (BAX, BAK, etc.). The ratio between these anti-apoptotic and proapoptotic members of the BCL-2 family helps determine the sensitivity of cells to the death signal.[94] Accordingly, the rate of change between them was analyzed by RT-PCR. Statistical analysis was performed by proportioning the gene expression levels (at the transcript level) of the proapoptotic gene BAX and the antiapoptotic gene BCL-2. BAX gene expression level increases in cells that will go to the apoptosis pathway, while BCL-2 gene expression level decreases.[95–98] In our study, in comparison with the control, there was no significant increase in BAX/BCL2 ratio in the group given 10 μg/ml Tmab, but a significant increase in BAX/BCL2 ratio was observed in the 10 μg/ml Tmab + 50 μM LND-NP. The most significant increase was seen in the combination with 10 μg/ml Tmab + 50 μM LND-NP, which showed a ***14-fold increase*** compared to the control. According to these results, induced apoptosis was confirmed by Annexin V and RT-PCR results. In terms of the contribution of our study to the literature, induced apoptotic cells are formed with the combination of a targeted nanoparticle with Tmab and it gives a more effective result than the use of LND alone. In our study, all groups were used, and each was compared with Tmab and LND NP.

4. Conclusions

Our study involves targeted inhibition of glycolysis of the HK2 enzyme and targeted inhibition of the overexpressed HER2 pathway. With combined inhibition of these two targets, reduced survival, negative metastasis, and induced apoptosis are expected to be observed. For this purpose, Tmab, LND and LND loaded NPs were used. Lonidamine causes toxic effects when administered alone. Here, Lonidamine, which is sent to the cell with the help of nanoparticles, makes a targeting thanks to the size of the nanoparticles and shows its effectiveness in that region for a long time. While Lonidamine alone gives an IC50 value of 124.6 μM, LND applied with NP gives an IC50 value of 44.18 μM. Thanks to NP, the IC50 value decreases approximately 3 times. This clearly shows that nanoparticle systems can cause positive effects in terms of toxicity. In this context, it has been shown by different molecular experiments that the combination of 10 μg/ml Tmab + 50 μM LND-NP induces apoptosis. When all parameters were examined, it was seen that the combination of 10 μg/ml Tmab + 50 μM LND-NP increased apoptosis. Our study presents the molecular mechanisms by which Tmab, an effective drug in breast cancer, and LND-loaded hybrid NPs may be an effective combination therapy in chemotherapy. Our study needs to be supported by in vivo experiments and efficacy studies. If the results of these experiments are promising, HER2-positive cancer patients may be offered an important chemotherapy opportunity.

Author's Contributions

CRediT authorship contribution statement for this manuscript is described below. ***Fatma Ozlem Zurnaci (FOZ)***: Conceptualiza-

tion, data curation, formal analysis, investigation, methodology, validation, writing-original draft. ***Sukran Ozdatli Kurtulus (SOK):*** Conceptualization, formal analysis, methodology, validation. ***Ceyda Tuba Sengel Turk (CTST):*** Data curation, formal analysis, methodology, software, writing-original draft. ***Canan Hascicek (CH):*** Methodology, supervision, writing -original draft. ***Mustafa Guzel (MG):*** Conceptualization, investigation, methodology, supervision, visualization, resources, writing –original draft, writing –review & editing.

Acknowledgements

The authors sincerely thank Dr. Serife Yerlikaya for her assistance in the Annexin V and Real Time PCR studies. In addition, the authors thank Arven Pharma for their support. The authors declare that is no financial support for this research.

Conflict of Interests

The authors declare no conflict of interest.

Data Availability Statement

The data that support the findings of this study are available in the supplementary material of this article.

Keywords: Apoptosis · Cancer · Lonidamine · Nanoparticle · and Trastuzumab

[1] N. Azamjah, Y. Soltan-Zadeh, F. Zayeri, *Asian Pac. J. Cancer Prev.* **2019**, *20*, 7.
[2] M. D. Brooks, M. L. Burness, M. S. Wicha, *Cell Stem Cell* **2015**, *17*, 3 .
[3] M. Cianfrocca, W. Gradishar, *CA Cancer J. Clin.* **2009**, *59*, 303–313.
[4] A. Goldhirsch, E. P. Winer, A. S. Coates, R. D. Gelber, M. Piccart-Gebhart, B. Thürlimann *et al. Ann. Oncol.* **2013**, *24*, 2206–2223.
[5] J. Ross, E. Slodkowska, W. Symmans, L. Pusztai, P. Ravdin, G. Hortobagyi, *Oncologist* **2009**, *14*, 320–68.
[6] J. Ross, E. Slodkowska, W. Symmans, L. Pusztai, P. Ravdin, G. Hortobagyi, *Oncologist* **2009**, *14*, 320–68.
[7] I. L. Andrulis, S. B. Bull, M. E. Blackstein, D. Sutherland, C. Mak, S. Sidlofsky et al, *J. Clin. Oncol.* **1998**, *16*, 4.
[8] U. Krishnamurti, J. F. Silverman, *Adv. Anat. Pathol.* **2014**, *21*, 100–107.
[9] E. Li, K. Hristova, *Cell Adhesion Migration* **2022**, *4*, 249–254.
[10] M. M. Moasser, *Oncogene* **2007**, *26*, 6469–6487.
[11] Y. Feng, M. Spezia, S. Huang, C. Yuan, Z. Zeng, L. Zhang et al Genes, *Diseases* **2018**, *5*, 77–106.
[12] E. Van Raemdonck, G. Floris, P. Berteloot, A. Laenen, I. Vergote, H. Wildiers *et al. Breast Cancer Res Treat.* **2020**, *185*, 183–194.
[13] E. Van Raemdonck, G. Floris, P. Berteloot, A. Laenen, I. Vergote, H. Wildiers *et al. Breast Cancer Res Treat.* **2020**.
[14] Z. X. Yao, L. J. Lu, R. J. Wang, J. L. Bin, S. C. Liu, H. Y. Li *et al. Med Oncol.* **2014**, *31*, 798.
[15] N. Iqbal, *Mol. Biol. Int.* **2014**, *9*, 852748.
[16] Z. Q. Xu, Y. Zhang, N. Li, P. J. Liu, L. Gao, X. Gao *et al. BMJ Open* **2017**, 17.
[17] J. P. Spano, D. Azria, A. Gonçalves, *Crit. Rev. Oncol. Hematol.* **2015**, *94*.
[18] M. A. Cobleigh, C. L. Vogel, D. Tripathy, N. J. Robert, S. Scholl, L. Fehrenbacher, *et al. J. Clin. Oncol.* **1999**, *17*.
[19] C. L. Vogel, M. A. Cobleigh, D. Tripathy, J. C. Gutheil, L. N. Harris, L. Fehrenbacher, *et al. J. Clin. Oncol.* **2002**, *20*.
[20] J. Baselga, X. Carbonell, N. J. Castañeda-Soto, M. Clemens, M. Green, V. Harvey *et al. J. Clin. Oncol.* **2005**, *23*.
[21] H. Rugo, M. Brammer, F. Zhang, D. Lalla, *Clin. Breast Cancer* **2010**, *10*.
[22] B. Leyland-Jones, K. Gelmon, J. P. Ayoub, A. Arnold, S. Verma, R. Dias *et al. J. Clin. Oncol.* **2003**, *21*, 22–46.
[23] P. R. Pohlmann, I. A. Mayer, R. Mernaugh, *Clin. Cancer Res.* **2009**, *15*.
[24] D. C. Roopenian, S. Akilesh, *Nat. Rev. Immunol.* **2007**, *7*.
[25] J. Baselga, *Semin. Oncol.* **2001**, *28*.
[26] S. Lei, J. Yang, C. Chen, J. Sun, L. Yang, H. Tang *et al. J. Exp. Clin. Cancer Res.* **2016**, *35*.
[27] X. S. Chen, L. Y. Li, Y. D. Guan, J. M. Yang, Y. Cheng, *Acta Pharmacologica Sinica.* **2016**, *37*.
[28] A. Boiteux, B. Hess, *Philos. Trans. Royal Soc. Lond.* **1981**, *293*.
[29] M. Saraswat, T. Mrudula, P. U. Kumar, A. Suneetha, T. S. Rao, M. Srinivasulu, *Med. Sci. Monitor* **2006**, *12*.
[30] V. L. Zinsser, E. M. Hoey, A. Trudgett, D. J. Timson, *Biochimie* **2013**, *95*.
[31] T. Chen, Z. Huang, Y. Tian, B. Lin, R. He, H. Wang *et al. Medicine (US)* **2017**, *96*.
[32] T. Hitosugi, L. Zhou, S. Elf, J. Fan, H. B. Kang, J. H. Seo, et al. *Cancer Cell.* **2012**, *22*.
[33] T. M. Larsen, J. E. Wedekind, I. Rayment, G. H. Reed, *Biochemistry* **1996**, *35*.
[34] G. C. Chang, K. J. Liu, C. L. Hsieh, T. S. Hu, S. Charoenfuprasert, H. K. Liu et al, *Clin. Cancer Res.* **2006**, *12*.
[35] T. Park, Y. J. Lee, S. H. Jeong, S. K. Choi, E. J. Jung, Y. T. Ju et al, *J. Gastric Cancer.* **2017**, *17*.
[36] F. Sharif, A. Rasul, A. Ashraf, G. Hussain, T. Younis, I. Sarfraz, *et al. IUBMB Life* **2019**, *71*.
[37] M. Akram, *J. Cancer Educ.* **2013**, *28*.
[38] T. Zhang, X. Zhu, H. Wu, K. Jiang, G. Zhao, A. Shaukat, *et al., J. Cell Mol. Med.* **2019**, *23*.
[39] S. N. Garcia, R. C. Guedes, M. M. Marques, *Curr. Med. Chem.* **2018**, *26*.
[40] Z. Chen, W. Lu, C. Garcia-Prieto, P. Huang, *J. Bioenerg. Biomembr.* **2007**, *39*.
[41] S. Li, J. Li, W. Dai, Q. Zhang, J. Feng, L. Wu, *et al. Br. J. Cancer.* **2017**, *117*.
[42] H. J. Lee, C. F. Li, D. Ruan, J. He, E. D. Montal, S. Lorenz *et al. Nat Commun.* **2019**, *10*, 1–16.
[43] N. Hay, *Nat. Rev. Cancer.* **2016**, *16*.
[44] N. Ho, B. L. Coomber, *Cancer Treat Commun.* **2016**, *6*.
[45] F. Xi, J. Ye, *Oncol. Res.* **2016**, *23*.
[46] A. Mukherjee, Y. Ma, F. Yuan, Y. Gong, Z. Fang, E. M. Mohamed et al, *Neoplasia (US)* **2015**, *17*.
[47] Lis, P., Dyląg, M., Niedźwiecka, K., Ko, Y. H., Pedersen, P. L., Goffeau, A., & Ułaszewski, S. (2016). The HK2 dependent "Warburg effect" and mitochondrial oxidative phosphorylation in cancer: targets for effective therapy with 3-bromopyruvate. Molecules, 21(12), 1730. .
[48] W. Li, M. Zheng, S. Wu, S. Gao, M. Yang, Z. Li, *et al. J. Exp. Clin. Cancer Res.* **2017**, *36*, 1–12.
[49] Y. Guo, X. Liu, Y. Zhang, H. Qiu, F. Ouyang, Y. He, *Life Sci.* **2020**, *256*.
[50] R. Scatena, P. Bottoni, A. Pontoglio, L. Mastrototaro, B. Giardina, *Expert Opin. Investig. Drugs* **2008**, *17*.
[51] G. S. Price, R. L. Page, J. E. Riviere, J. M. Cline, D. E. Thrall, *Cancer Chemother. Pharmacol.* **1996**, *38*.
[52] X. Chen, L. Wei, L. Yang, W. Guo, Q. Guo, Y. Zhou, *Food Chem. Toxicol.* **2020**, *143*.
[53] W. M. Rosencrans, M. Rajendran, S. M. Bezrukov, T. K. Rostovtseva, *Cell Calcium.* **2021**, *94*.
[54] J. Pastorino, J. Hoek, *Curr. Med. Chem.* **2005**, *10*.
[55] M. Rho, J. Kim, D. J. Chang, M. L. You, E. L. Hee, M. A. Kim, *et al., Anticancer Res.* **2007**, *27*.
[56] J. G. Pastorino, J. B. Hoek, *J. Bioenerg. Biomembr.* **2008**, *40*.
[57] J. G. P. J. B. Hoek, *J. Bioenerg. Biomembr.* **2008**, *40*, 171–82.
[58] S. Ben-Haim, P. Ell, *J. Nucl. Med.* **2009**, *50*.
[59] K. McLarty, B. Cornelissen, Z. Cai, D. A. Scollard, D. L. Costantini, S. J. Done, *J. Nucl. Med.* **2009**, *50*.
[60] N. Jura, Y. Shan, X. Cao, D. E. Shaw, J. Kuriyan, *Proc. Natl. Acad. Sci. U S A* **2009**, *106*.
[61] R. W. Cheyne, L. Trembleau, A. McLaughlin, T. A. D. Smith, *Nucl. Med. Biol.* **2011**, *38*.
[62] T. A. D. Smith, M. V. C. L. Appleyard, S. Sharp, I. N. Fleming, K. Murray, A. M. Thompson, *Cancer Chemother. Pharmacol.* **2013**, *71*.
[63] A. Moreno-Aspitia, E. M. Holmes, C. Jackisch, E. De Azambuja, F. M. Boyle, D. W. Hillman, *J. Clin. Oncol.* **2017**, *35*.
[64] L. Ding, C. Tian, S. Feng, G. Fida, C. Zhang, Y. Ma *et al. Theranostics* **2015**, *5*.

[65] C. Tian, Z. Yuan, D. Xu, P. Ding, T. Wang, L. Zhang et al, *Exp. Cell Res.* **2017**, *357*.
[66] Q. Zuo, J. Liu, J. Zhang, M. Wu, L. Guo, W. Liao, *Sci. Rep.* **2015**, *5*.
[67] J. Liu, C. Pan, L. Guo, M. Wu, J. Guo, S. Peng *et al. J. Hematol. Oncol.* **2016**, *9*.
[68] B. Liu, Z. Fan, S. M. Edgerton, X. Yang, S. E. Lind, A. D. Thor *Cell Cycle* **2011**, *10*.
[69] N. Takahashi, K. Furuta, H. Taniguchi, Y. Sasaki, H. Shoji, Y. Honma *et al. Oncotarget* **2016**, 7.
[70] B. Salani, A. Del Rio, C. Marini, G. Sambuceti, R. Cordera, D. Maggi, *Endocr. Relat. Cancer* **2014**, *21*.
[71] C. T. Shen, W. J. Wei, Z. L. Qiu, H. J. Song, X. Y. Zhang, Z. K. Sun, *J. Mol. Endocrinol.* **2017**, *58*.
[72] D. W. Deamer, *FASEB J.* **2010**, *24*.
[73] T. M. Allen, P. R. Cullis, *Adv. Drug Deliv. Rev.* **2013**, *65*.
[74] W. T. Al-Jamal, K. Kostarelos, *Acc. Chem. Res.* **2011**, *44*.
[75] C. T. Sengel-Turk, N. Ozmen, F. Bakar-Ates, *Polym. Bulletin.* **2021**, *78*.
[76] C. T. Sengel-Turk, C. Hascicek, *J. Drug Deliv. Sci. Technol.* **2017**, *39*.
[77] X. Song, Y. Zhao, W. Wu, Y. Bi, Z. Cai, Q. Chen *et al. Int. J. Pharm.* **2008**, *350*.
[78] C. T. Şengel-Türk, C. Hasçiçek, A. L. Dogan, G. Esendagli, D. Guc, N. Gönül, *Drug Dev. Ind. Pharm.* **2012**, *38*.
[79] A. Budhian, S. J. Siegel, K. I. Winey, *Int. J. Pharm.* **2007**, *336*.
[80] S. P. Kennedy, M. O'Neill, D. Cunningham, P. G. Morris, S. Toomey, C. Blanco-Aparicio *et al. Oncogene* **2020**, *39*.
[81] X. Chen, H. Wang, X. N. Ou-Yang, F. W. Xie, J. J. Wu, *Wspolczesna Onkologia* **2013**, *17*.
[82] T. Fujita, H. Doihara, K. Kawasaki, D. Takabatake, H. Takahashi, K. Washio *et al. Br. J. Cancer* **2006**, *94*.
[83] N. Normanno, M. Campiglio, A. De Luca, G. Somenzi, M. Maiello, F. Ciardiello *et al. Ann. Oncol.* **2002**, *13*.
[84] S. Y. Kim, H. P. Kim, Y. J. Kim, D. Y. Oh, S. A. Im, D. Lee *et al. Int. J. Oncol.* **2008**, *32*.
[85] T. V. Komarova, E. V. Sheshukova, E. N. Kosobokova, V. S. Kosorukov, A. V. Shindyapina, F. A. Lipskerov *et al. Sci. Rep.* **2019**, *9*.
[86] S. Zazo, P. González-Alonso, E. Martín-Aparicio, C. Chamizo, I. Cristóbal, O. Arpí, *et al. Am. J. Cancer Res.* **2016**, *6*.
[87] F. Morais-Santos, V. Miranda-Gonçalves, S. Pinheiro, A. F. Vieira, J. Paredes, F. C. Schmitt, *et al. Endocr. Relat. Cancer* **2014**, *21*.
[88] Y. Huang, G. Sun, X. Sun, F. Li, L. Zhao, R. Zhong, *Cancers.* **2020**, *12*(11), 3332
[89] E. Calvino, M. C. Estañ, G. P. Simon, P. Sancho, M. del Carmen Boyano-Adanez, E. de Blas, *Biochem Pharmacol.* **2011**, *82*(11), 1619–1629
[90] G. S. Krasnov, A. A. Dmitriev, V. A. Lakunina, A. A Kirpiy, A. V. Kudryavtseva, *Expert Opin Ther Targets.* **2013**, *17*(10), 1221–1233.
[91] J. An, M. S. Sheikh, *Curr Cancer Drug Targets.* **2019**, *19*(5), 400–407.
[92] C. Bernard-Marty, F. Lebrun, A. Awada, M. J. Piccart, *Monoclonal, Drugs.* **2006**, *66*, 1577–1591.
[93] R. Nahta, *ISRN Oncol.* **2012**, *2012*.
[94] M. S. Ola, M. Nawaz, H. Ahsan, *Mol Cell Biochem.* **2011**, *351*, 41–58
[95] C. Spampanato, S. De Maria, M. Sarnataro, E. Giordano, M. Zanfardino, S. Baiano, *Int J Oncol.* **2012**, *40*(4), 935–941
[96] R. C. Bargou, P. T. Daniel, M. Y. Mapara, K. Bommert, C. Wagener, B. Kallinich, *Int J Cancer.* **1995**, *60*(6), 854–859
[97] E. Khodapasand, N. Jafarzadeh, F. Farrokhi, B. Kamalidehghan, M. Houshmand, *J. Iran Biomed* **2015**, *19*(2), 69.
[98] S. Aggarwal, S. Gupta, **1998**, *160(4)*, 1627–1637.

Manuscript received: November 12, 2023